ORIGINAL ARTICLE

Drag force on micron-sized objects with different surface morphologies in a flow with a small Reynolds number

Arif Md. Rashedul Kabir[1], Daisuke Inoue[2], Yuri Kishimoto[3], Jun-ichi Hotta[4], Keiji Sasaki[5], Noboru Kitamura[1], Jian Ping Gong[6], Hiroyuki Mayama[7] and Akira Kakugo[1,2]

The lack of a suitable experimental setup and a limited number of *in vitro* investigations have impeded understanding of the factors that have important roles in altering the drag force acting on tiny microobjects in a fluidic medium. Here we investigated how the surface morphology affects the drag force acting on microparticles. The drag coefficient for micron-sized polymer-grafted polystyrene (PS) and negatively charged hard (silica) and soft (hydrogel) spheres were evaluated and compared with that of a PS particle. The drag coefficient of the PS particle was found to be comparable to that predicted according to the Stokes' formula for a hard sphere. By contrast, polymer-grafted PS and negatively charged hard and soft spheres showed a considerable deviation from the Stokes' formula. The drag coefficient decreased by ~60 and ~86% for the negatively charged hard and soft spheres, respectively, whereas it increased by ~20% for the polymer-grafted PS particles with respect to that of the PS particle. This work reveals the role of the surface morphology of small objects in altering the drag force acting on them; such knowledge may help elucidate the mechanism by which the surface morphology of aquatic microorganisms helps them to control the drag force, which consequently might facilitate the invention of new technologies for micromachines or microdevices.

INTRODUCTION

Drag force always acts on objects in flow, and its magnitude depends on both the geometry of flow around the objects and the Reynolds number; the Reynolds number is well-known as the ratio of the force of inertia to the viscous force.[1] On the one hand, for a massive ocean liner, the force of inertia dominates over the Reynolds number (Re), that is, Re≫1. On the other hand, for small objects, such as a bacterium, the viscous force dominates over the Re, and Re≪1. In this case, it is the drag that opposes the object's acceleration.[1] In nature, the drag-reduction ability of aquatic animals and microorganisms has evolved to realize improved efficiency and/or speed and to harness a favorable energy benefit in swimming; therefore, drag reduction is closely related to their survival in an adverse environment.[2–4] Several factors, such as size, shape, surface morphology and so on, are known to influence the drag reduction of aquatic animals, which is achieved mainly through a skin-friction drag-reduction strategy.[5–13] In nature, skin-friction drag reduction is accomplished through two approaches: (i) body smoothness or alteration of the structure of turbulent motions and (ii) maintenance of laminar flow using smooth surfaces and favorable pressure gradients. For example, most fish slimes that contain high-molecular weight polymer compounds and surfactants

can exhibit significant drag-reduction behavior.[14–18] In addition, bubble-mediated drag reduction has been noted in the case of seals and penguins and so on that travel near and through the air–water interface.[19] Laboratory studies have also suggested that different types of surface additives, such as polymers, surfactants and bubbles, can provide the largest skin-friction drag reduction in water.[20] Bubbles were reported to decrease the average density near the wall and have an efficient role in drag reduction by more than ~50%.[5] Moreover, skin-friction drag reduction is sometimes accomplished by surface and body-geometry modifications, as observed in the cases of swordfish and sharks.[6,7,9,10] Thus, a comprehensive level of knowledge has already been acquired about the drag-reduction technique of aquatic animals (Re≫1). By contrast, understanding the drag reduction by microorganisms corresponding to low Reynolds numbers, although also of considerable interest, requires further study. Such study may lead to the invention of technologies for practical applications via understanding and mimicking animal forms and functions in nature. However, there has been a longstanding mystery regarding the survival mechanism of small organisms (Re≪1). In spite of the drag force acting on them, the microorganisms can move and adapt to an adverse environment, which is believed to be achieved through alteration of

[1]Faculty of Science, Hokkaido University, Sapporo, Japan; [2]Graduate School of Chemical Sciences and Engineering, Hokkaido University, Sapporo, Japan; [3]Graduate School of Science, Hokkaido University, Sapporo, Japan; [4]Graduate School of Science and Engineering, Yamagata University, Yonezawa, Japan; [5]Research Institute for Electronic Science, Hokkaido University, Sapporo, Japan; [6]Faculty of Advanced Life Science, Hokkaido University, Sapporo, Japan and [7]Department of Chemistry, Asahikawa Medical University, Asahikawa, Japan
Correspondence: Professor A Kakugo, Graduate School of Chemical Sciences and Engineering, Hokkaido University, Sapporo 060-0810, Japan.
E-mail: kakugo@sci.hokudai.ac.jp

the drag coefficient, that is, the drag force acting on them. Limited in vitro studies on the drag reduction of small organisms, due to the lack of availability of a suitable experimental technique, has been the problem in this regard. Therefore, in this work, we experimentally investigated the drag coefficient of small objects (microparticles) with different sizes and surface morphologies. For this work, we developed an experimental setup that can be used to measure the drag force acting on microparticles in an aqueous medium. Our work clearly reveals that the surface morphology of microparticles has an important role in altering the drag force acting on them. Moreover, based on our observations, surface roughness and surface charge are also suspected to affect the drag force working on the microparticles. This work would be helpful in elucidating the mechanism behind alteration of the drag force acting on aquatic microorganisms in nature, which in turn would be important for developing new technologies that may find potential applications in future artificial micromachines or smart microdevices.

EXPERIMENTAL PROCEDURE

Materials

Styrene (St; Junsei Chemical, Tokyo, Japan) was distilled under reduced pressure. Vinylbenzenechloride (VBC; Tokyo Chemical Industry, Tokyo, Japan) was washed with 0.5% NaOH and H_2O, and then distilled under reduced pressure. 2-Acrylamide-2-methylpropane sulfonic acid (AMPS; Tokyo Chemical Industry, Tokyo, Japan) was recrystallized from methanol. Acrylamide (Junsei Chemical, Tokyo, Japan) was recrystallized from chloroform. Divinylbenzene (55%; Wako Pure Chemical Industries, Osaka, Japan) was used as received. 2,2-methylenebisacrylamide (Kanto Chemical, Tokyo, Japan) was recrystallized in ethanol. Sodium-N,N-diethylthiocarbamate (Sigma-Aldrich Japan KK, Tokyo, Japan) was used as received. 2,2′-Azobis (isobutyronitrile) (Wako Pure Chemical Industries, Osaka, Japan) was recrystallized from water. Potassium peroxydisulfate (Kanto Chemical, Tokyo, Japan) was recrystallized from water. N,N,N′,N′-tetramethylethylenediamine (Tokyo Chemical Industry, Tokyo, Japan) was used as received. Polyvinylpyrrolidone (Junsei Chemical, Tokyo, Japan), sorbitan monoleate (span85; Kanto Chemical, Tokyo, Japan) and sodium dodecyl sulfate (SDS; Wako Pure Chemical Industries, Osaka, Japan) were used as received. Polystyrene (PS) beads and silica beads (Catalysts & Chemicals Industries, Yokohama, Japan) were washed with 20 wt% KOH solution and dispersed in water (pH ~ 7.0) until use.

Preparation of PS beads

PS beads were prepared according to the protocol described in the literature.[21] Polymerization of St was performed in a 100-ml three-necked round-bottom flask by stirring with a four-bladed metal stirrer and passing a nitrogen gas flow through the flask to maintain an inert atmosphere. The total charged weight, including the initiator and solvent, was 50 g. The reaction temperature was controlled by placing the flask in a water bath at 70 °C. The reaction mixture (St 35 wt%, ethanol 35 wt% of total weight, divinylbenzene 0.5 wt%, polyvinylpyrrolidone 25 wt% and dimethylformamide 20 wt% of St) was stirred at 85 r.p.m. for 30 min. Next, the initiator solution (2,2′-Azobis(isobutyronitrile) 5.0 wt% of St, ethanol 20 wt% of total weight) was added to polymerize the St monomers by stirring the mixture at 50 r.p.m. for 15 h. The resulting PS particles were collected by centrifugation and then washed with ethanol; this process was repeated five times, followed by washing five times with water.

Preparation of polyacrylamide (PAAm)-grafted particles

PAAm-grafted particles were prepared according to the protocol described in the literature.[22] First, core particles with benzylchloride groups on the surface were prepared via copolymerization of St and VBC in a three-necked round-bottom flask in an inert atmosphere as described above. The total charged weight, including the initiator and solvent, was 25 g. The reaction temperature was controlled by placing the flask in a water bath at 70 °C. The reaction mixture (St 35 wt%, ethanol 40 wt% of total weight, polyvinylpyrrolidone

2.5 wt% and dimethylformamide 20 wt% of St) was stirred at 60 r.p.m. for 30 min. Next, the initiator solution (2,2′-Azobis(isobutyronitrile) 5.0 wt% of St and ethanol 50 wt% of total weight) was added, and then the mixture was stirred at 50 r.p.m. for 4 h. During polymerization, divinylbenzene of 0.5 wt% of St and ethanol 6.0 wt% of total weight was added to the mixture at a rate of 1 drop/min. The resulting core particles were collected by centrifugation and then washed with ethanol; this process was repeated five times, followed by washing five times with water. Next, iniferter fragments were immobilized on the surface of core particles via the NaCl elimination reaction between sodium-N,N-diethylthiocarbamate and the benzylchloride group on the particle. A unit of 50 g of 0.2 wt% of the core particles in water were charged into a 100-ml three-necked round-bottom flask in a cold bath filled with ice. A unit of 30 g of 3.7 wt% sodium-N,N-diethylthiocarbamate solution was added dropwise for 30 min to the gently agitated core particle solution. Subsequently, the reaction was continued at room temperature for 30 h to immobilize dithiocarbamate on the particles. The resulting particles, named as 'VBC–diethylthiocarbamate', were collected and washed as described above. The modification ratio of sodium-N,N-diethylthiocarbamate was estimated by elemental analysis. Next, PAAm-grafted particles were prepared using the iniferter polymerization reaction. A unit of 50 g of reaction mixture was prepared by dissolving 0.02 g of VBC–diethylthiocarbamate and 2 g of acrylamide in a mixture of dimethylformamide (63%) and water (37%). The mixture was charged in a 100-ml three-necked round-bottom flask and exposed to ultraviolet (365 nm) irradiation using a mercury lamp. The acrylamide-grafted particles thus obtained were named 'PAAm–VBC' and were washed by water and collected by centrifugation. The molecular weight of each acrylamide-grafted particle was estimated using 'gel permeation chromatography' by measuring the molecular weight of the polymers synthesized by polymerization via suspended initiators in the bulk solution. The molecular weight of the polymers grafted on the particle surface was ~ 10^5, as measured by gel permeation chromatography with polyethylene glycol used as the standard.

Preparation of PAAm–methylpropane sulfonic acid (PAMPS) gel particle

A 50 ml solution containing 0.5 M 2-acrylamide-2-methylpropane sulfonic acid, 10 mol% 2,2-methylenebisacrylamide and 1.0 mol% potassium peroxydisulfate was mixed with 3.3 ml span85 and 40 ml of toluene in a flask and stirred for 30 min at 500 r.p.m. at an argon atmosphere. Next, 2.9 µl of N,N,N′, N′-tetramethylethylenediamine was added, and the reaction was allowed to continue for 3 h. The resulting PAMPS gel particles were collected by centrifugation and then washed with toluene three times and with water five times.

Characterization of the particles

The zeta potential of the particles prepared was measured using a zeta potential measurement device MARK2 (Central Scientific Commerce, Tokyo, Japan). The surface morphology of the particles was investigated using scanning electron microscopy (S-2250N; Hitachi, Tokyo, Japan). The size of the particles was characterized by microscopic observation using a × 100 objective lens.

Flow channel (microchannel) preparation

Glass coverslips and polydimethylsiloxane were used as the substrate and material, respectively, for preparing the flow channel based on the conventional technique described in the literature.[23–25] First, a photomask was prepared by using a positive photoresist (OFPR800; Tokyo Ohka Kogyo, Kanagawa, Japan). The surface of a chromium-coated cover glass was coated with the photoresist by spin-coating at 1000 r.p.m. for 5 min and then baked at 110 °C for 90 s. By using an overhead projection film photomask, an area of the cover glass (0.5 × 40.0 mm) was then exposed to light from a halogen lamp (300 W) for 90 s. The cover glass was immersed in NMD-3(aq.), a developer solvent, to lift off the light-exposed area. Finally, the cover glass was washed with water, postbaked for 5 min at 110 °C, immersed in a 10% aqueous solution of cerium (IV) ammonium nitrate for etching chromium and then washed with ethanol to remove residual photoresist. Next, the channel template was prepared on a cover glass by using negative photoresist SU-8 (MicroChem; Westborough, MA, USA) and the prepared photomask under exposure to the light from a

halogen lamp (300 W) for 5.5 min. The mold was prepared by immersing in a developer for 6 min. Polydimethylsiloxane prepolymer Sylgard 184 (Dow Corning, MI, USA) was mixed with the crosslinker, Silpot 184 (Dow Corning, MI, USA) at a weight ratio of 10:1 and was poured onto the mold, followed by curing at 65 °C for 1 h. The obtained polydimethylsiloxane replica (40.0 mm × 1150 μm × 120.0 μm) was peeled off from the mold and placed onto a cover glass. Using epoxy-type glue, a silica capillary tube (inner diameter 0.1 mm and outer diameter 0.2 mm; GL Sciences, Tokyo, Japan) was placed to connect it to the end of the flow channel, as shown schematically in Figure 1. The other end of the capillary tube was connected to a microsyringe (Hamilton Gastight syringes, 50 μl) and fixed to a micropump (Harvard PHD 4400 remote programmable 70–2201; Harvard Apparatus, Holliston, MA, USA) to provide a steady flow of buffer.

Measurement of the drag force acting on the particles

Stokes' formula regarding the measurement of the drag force acting on a small particle in any fluidic medium was used; the formula is given below:

$$F = 6\pi\eta rv$$

where F, η, r and v are the drag force exerted on particle, the viscosity of the medium, the radius of the particle and the velocity of particle, respectively. As schematically shown in Figure 1, the drag force on the microparticles was measured by using thermodynamic analysis of the Brownian motion of the particles that were trapped by the radiation pressure induced by an optical force.[26–29] Microparticles dispersed in the channel were optically trapped by a focused 1064-nm beam of a CW Nd:YAG laser (10 mW) under an optical microscope (Nikon TE2000; Nikon Instruments Inc., Melville, NY, USA). The particle position was controlled by a laser manipulator instrument (LM-02; Tokyo Instruments, Tokyo, Japan). Brownian motion of the particle was detected by collecting and monitoring the scattered light from the particle through an objective lens by using a quadrant photodiode (S4349; Hamamatsu Photonics KK, Shizouka, Japan) under a dark-field microscope. Four output signals from the quadrant photodiode were transmitted to a computer (Epson endeavor pro 3300) via a BNC terminal block (BNC-2110; National Instruments Corporation, Austin, TX, USA) for data acquisition. The force measurement was performed with the aid of software (molecular force measurement, MFM version 4.16; Tokyo Instruments, Tokyo, Japan). The sampling number and frequency for detecting the position of the particles were 2 500 000 and 0.1 MHz, respectively. The measurement of the drag force was performed at least three times for each case, and then the values were averaged. In this work, the suspending medium was an aqueous medium, and Milli-Q water (EMD Millipore, Billerica, MA, USA) of resistivity of 1.82×10^5 Ωm was used. To minimize the wall effect, we measured the drag force at the center of the microchannel, with 100 nm accuracy, that is, at a position equidistant from the channel wall along the y- and z-axes, where the x-axis denotes the direction along the length of the flow channel. All the experiments in this work were performed at 25 °C.

Note that we considered the same PS particle for each of the prescribed sizes for measuring drag force acting on the particle at different flow velocities and confirmed the reliability of our data by repeating each experiment several times. The same methodology was also applied for measuring the drag force on different-sized particles with different surface morphologies. We performed a series of experiments using the same particle for each type of PS, silica, PAMPS and PAAm-grafted particles. Because the drag force on particles with different sizes and surface morphologies was measured one by one (one particle at a time), the variation in the particle size was not statistically considered here.

For characterizing the flow velocity–position profile of a particle, we used suspended particles, for example, mica or PS particles in the buffer and an optical microscope to trace the movement of the buffer (and particles) inside the flow channel. The flow velocity inside the flow channel was tuned by changing the flow rate of the buffer using a micropump. For measuring the flow velocity along the horizontal plane (the x–y plane), we focused on a position close to the substrate surface and then tracked the flow velocity, that is, the buffer flow induced movement of particles. We monitored the movement of suspended particles at different position of the flow channel along its y-axis (width) at that selected plane. For measuring the flow velocity along the vertical

direction (the x–z plane), the same procedure was used, but at a different position of the flow channel along the z-axis (height). Finally, the velocity was plotted against the position of the measurement.

RESULTS AND DISCUSSION

First, we studied the flow velocity–position profile of particles inside the microchannel. Figure 2 shows typical flow velocity–position profiles of the particles at the x–y and x–z planes inside the microchannel at an applied flow rate of 0.3 μl min^{-1}. As shown in this figure, the particle's position and flow velocity can be fitted in a plug flow profile in the x–y plane, and a parabolic profile in the x–z plane. Next, we studied the correlation between the applied flow rate and the flow velocity of particles while keeping the particle position fixed at 60 μm from the top/bottom surface of the substrate, that is, at the halfway point along the height of the channel (z-axis), and in the vicinity of the center along the width of the channel (y-axis). The flow velocity of particles inside the microchannel was linearly correlated to the applied flow rate within the range studied (data not shown). Considering the deviation from the mean value of flow velocity, we maintained the applied flow rate in the range of 0–0.3 μl min^{-1}. Next, the drag force on the PS particles (diameter, D, ~2.95 μm) was measured at different flow velocities by changing the applied flow rate to determine a suitable position for the drag force measurement. Figure 3 shows the dependence of the drag force exerted on the PS particles along the x- and y-directions. For measuring the drag force, first, we obtained both the x- and y-directional potentials exerted on a particle in the absence of any fluid flow as the reference. Next, we again collected the x- and y-directional potentials exerted on the particle in the presence of fluid flow of different velocities. From these data, the profiles of the energy difference between the two x- and two y-directional potentials (that is, with and without fluid flow) were obtained using a custom software package. The drag force on the particle was obtained from the slope of these potential curves, as described in a previous report.[26,27] We found that the drag force strongly depends on the x-position and that it can be described by Stokes' formula. In addition, the drag force along the y-position was almost constant. The position of the PS particle was manipulated using a galvanic mirror of the micromanipulator system to settle it at a position 60 μm away from the bottom of the microchannel and at the center along the width of the channel. With an increase in flow velocity, the drag force on the PS particles in the horizontal direction (x-axis) was found to increase linearly, as shown in Figure 3, although no change in drag force along the y-axis was observed. In this figure, the dotted line represents the drag force on a spherical solid particle calculated from Stokes' formula at different flow velocities. The change in drag force on the PS particles in the horizontal direction tends to follow the change according to Stokes' formula, although a slight deviation between the experimental results and the theoretically calculated values was observed. We suspect that such deviations might have arisen due to the deviation of the experimental conditions from those considered by Stokes' law. The present experimental situation for the PS particles is different from the ideal situation considered by Stokes' law, especially with respect to the surface charge of particles (see the discussion on zeta potential in a later section). Stokes' law assumes that a particle is a sphere with a smooth surface that has no surface charge. It is well-known that the distribution of counter ions in the vicinity of a charged surface obeys the Poisson–Boltzmann equation. However, the local viscosity of a fluid in the vicinity of the charged surface may slightly increase compared with the bulk viscosity due to relatively higher concentration of ions and clustering water molecules. This difference might be the primary reason behind
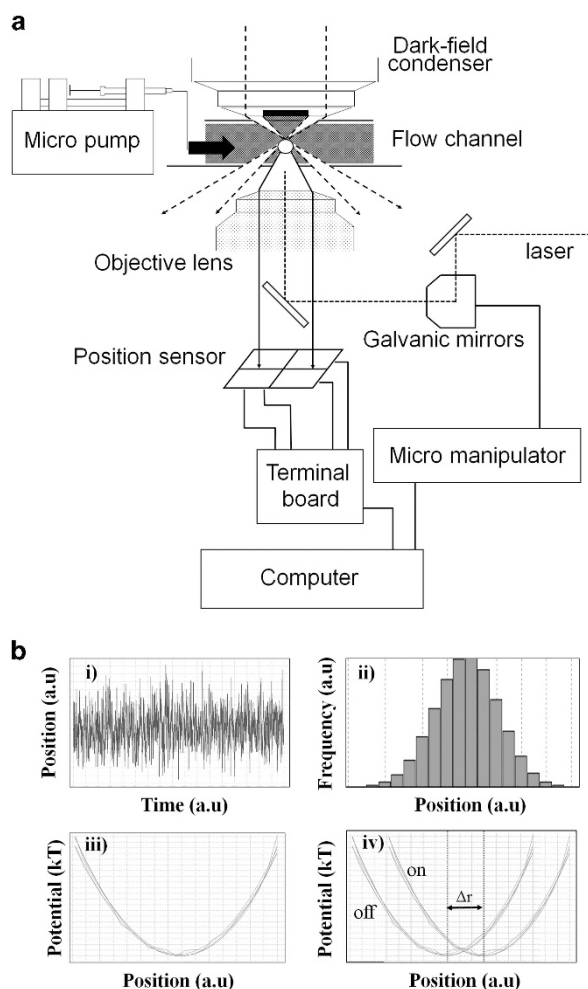
Figure 1 (a) Schematic representation of the experimental setup used to measure the drag force acting on microparticles in a microchannel. A dark-field microscope was used to monitor the microparticles inside the microchannel. (b) Typical figures illustrating the method of drag force determination: (i) time–position profile of a microparticle in the microchannel; (ii) histogram of the frequency of the different positions of the particle; (iii) potential exerted on the particle versus its position; and (iv) potentials exerted on the particle with (on) and without (off) an applied force. The applied force caused displacement of the curves, as indicated by 'Δr'. A full color version of this figure is available at Polymer Journal online.

the observed deviation in our experiment. Until now, although the effect of surface charge on small particles has been studied theoretically in electro-osmosis and electrokinetics using bulk viscosity, the importance of the local viscosity remains to be understood.[30–32] Next we studied the effect of particle size on the drag force acting on PS particles. Figure 4 shows the role of particle size on the force–velocity drag coefficient (drag force), where the drag coefficient was found to be proportional to the particle size; this result is in agreement with Stokes' formula within an experimental error. This result reveals that our drag force measurement system is applicable to detect the drag force inside the microchannel within a range of sub pN to several pN.

To understand the effect of the size and surface morphology, and so on, of moving bodies (microparticles) on the force–velocity drag coefficient, we prepared particles of varying sizes and surface morphologies. Figure 5 shows representative images of those synthesized particles with different surface morphologies. The sizes of the PS, silica and PAAm-grafted particles were in the range of 2–10 μm,

whereas those of the PAMPS gel particles were in the range of 500 nm–3 μm. The surfaces of the PS, silica and PAMPS gel particles were smooth or flat; however, a significant difference was observed in the case of PAAm-grafted particles, where the surface was found to be hairy/shaggy. For the PAAm-grafted particles, we considered the size of the particle core that was detectable under an optical microscope. However, we also roughly estimated the thickness of the hairy layer in terms of the size of the polymer. The polymer size 'R' of a Gaussian chain could be expressed as follows:

$$R = l_k N^{\frac{1}{2}}$$

Here l_k is the Kuhn length and N is the number of Kuhn segments in a polymer chain. In the present case, the average molecular weight is $\sim 10^5$ and the molecular weight of a monomer is 57; therefore, the polymerization number, n is 1.75×10^3. To calculate l_k and N in an individual PAAm chain, we assume that the angle and distance between C–C bonds are 109.5° and 1.54 Å, respectively; the length of the base of an isosceles triangle of -(CH$_2$-CH(CONH$_2$)-CH$_2$)$_n$- is 2.52 Å, the contour length of the individual polymer chains is 220 nm and the order of persistence length is 5 nm at most. Therefore, l_k and N are roughly estimated to be 10 nm and 22, respectively, and R is 50 nm. This rough estimation suggests that the thickness of the hairy polymer brush is negligibly small compared with the radius of the particle core. Thus, the effect of the hairy/shaggy polymer layer on the drag force of the PAAm-grafted particles was not considered.

Next, using these particles, we investigated how the size, surface morphology and physical property of particles, for example, softness, affected the drag coefficient, that is, the drag force exerted on them. As shown in Figure 5, the drag coefficient of the particles increased with increased particle size. Moreover, the drag coefficient of the particles was strongly affected by the surface morphology and the physical nature of the particles. When compared with the theoretically calculated values using the Stokes' law, the experimental data for different particles exhibited a considerable deviation. This result suggests that the surface morphology of the particles strongly affects the drag force exerted on them and, depending on the physical nature of the particles, shows a substantial level of deviation from the ideal conditions considered by Stokes' law. As already discussed, the data scatter in the presented cases could be accounted for due to the presence of surface charges, the particle's physical nature (for example, softness) and the change in the velocity of the fluid in the vicinity of the particle surface; further investigation in the future is required for confirmation. Table 1 lists the values of $F v^{-1} D^{-1}$ and the zeta potentials for different particles; here $F v^{-1} D^{-1}$ is a measure of drag coefficient per unit size for the particles. From this table, the drag coefficient per unit size for the silica and PAMPS gel particles were clearly smaller compared with that of the PS particles. More accurately, the drag coefficient per unit size decreased almost 60 and 86% for the silica and PAMPS gel particles with respect to that of the PS particles. In the case of PAAm-grafted particles, the drag coefficient per unit size increased ∼ 20% with respect to that of the PS particles.

One of the possible reasons behind the observed differences in the drag coefficient per unit size for different particles might be the change in their effective size. For PAAm-grafted particle, the inside of the particle is a hard sphere, and the grafting of polymer can increase the effective size of the hard sphere, thereby facilitating an increase in the coefficient. However, the change in the particle size due to polymer grafting was roughly estimated (discussed above), and the size change was found to be negligible compared with the core size of the particle. Therefore, other factors, for example, surface charge, might be involved in changing the drag coefficient. In the case of PAMPS gel
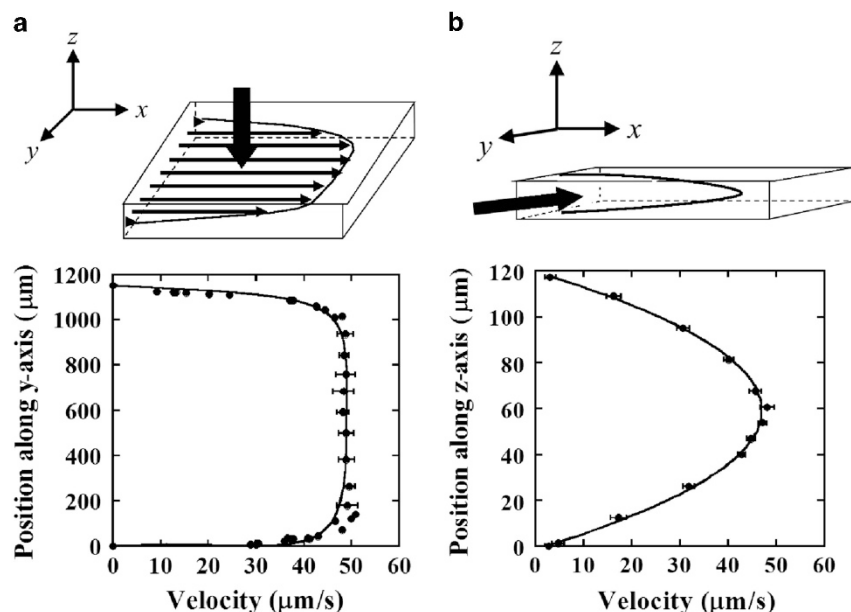
Figure 2 Flow velocity–position profile of a microparticle (polystyrene) at the (**a**) *x–y* plane and (**b**) *x–z* plane. The flow rate was maintained at 0.3 μl min^{-1}. The broad arrows indicate the direction of observation for monitoring the buffer flow inside the microchannel.
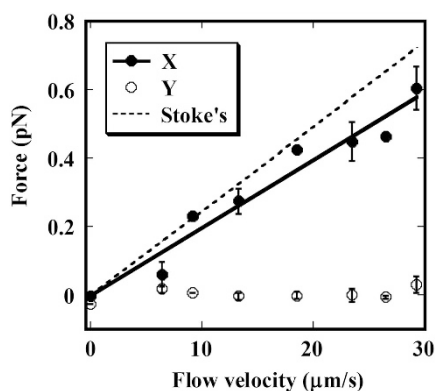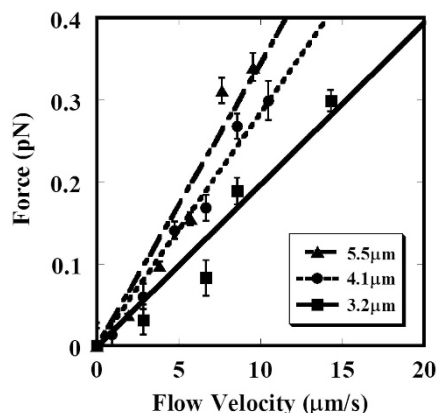

Figure 3 Change of the drag force on the polystyrene particle with the change of flow velocity. The drag force along the *x*-axis (closed circle) was increased linearly with the increase in flow velocity but remained almost constant along the *y*-axis (open circle). The straight lines were drawn according to the least-squares fit method.
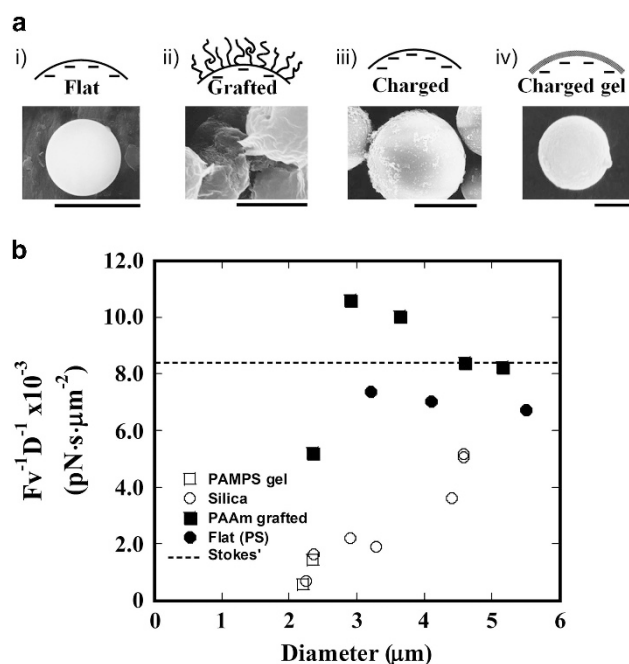
particles, the effective particle size may become smaller than the actual or apparent size of the gel particles, mainly because of the intrinsic properties of the gel material. Gel particles are primarily three-dimensional polymer networks containing >90% water; in addition, water from the surrounding can pass through the particle.[33] A decrease in the effective size might have played effective role in the reduction of the drag coefficient in this case. However, the reason behind the observed difference in the drag coefficient of PS and silica particles, despite their similar sizes, is not clear. To investigate this issue further, we measured the surface charge density (zeta potential) of the particles; the values are listed in Table 1. From the table, the zeta potential of the particles seems to be correlated to the drag coefficient per unit size, with a high zeta potential tending to decrease the drag coefficient. However, the extent of reduction of the drag coefficient per unit size may not be solely explained by the zeta potential, especially in the case of the gel particle, where the drag coefficient

decreased although the zeta potential was found to be nearly identical to that of the PS particle. In the future, further investigation is required to improve the understanding of the mechanism of the reduction of the drag coefficient.

Next, we discuss the relationship between the drag force and the surface morphology. To understand this relationship, the distribution of the velocity of fluid flow in the vicinity of surface of the body (microparticle) should be taken into account, with the velocity at the surface of the body considered to be zero. Figure 6 shows schematic illustrations of the microspheres of different surface morphologies in the microchannel. In Stokes' formula, the drag force is considered for a solid sphere with a smooth surface. In this case, the velocity of fluid flow in the vicinity of surface, *v* is proportional to the height (distance) from the solid surface, *h*. The boundary condition of $v(h) = 0$ represents the surface of the body (Figure 6a). In the case of the PAAm-grafted particle, the condition of $v(h) = 0$ can be considered at $h > 0$ due to the presence of the polymer chains, which makes the surface boundary unclear (Figure 6b). This possible increase in the effective radius, together with the role of the surface charge, could be considered as a possible explanation for the increase in the drag coefficient. However, the effective radius decreases in the case of the PAMPS gel particle. As previously mentioned, gel particles are three-dimensional polymer networks that allow water from the surroundings to pass through the particle. Thus, the condition of $v(h) = 0$ is fulfilled inside the gel ($h < 0$) instead of at the surface of the body, thereby decreasing the effective radius of the particle. This characteristic of hydrogel might be the reason why the drag coefficient of the gel particle decreased. Following this line of reasoning, the experimental result for silica suggests that the velocity at $h = 0$ is not equal to zero, that is, $v(h = 0) \neq 0$. The friction between the negatively charged surface and water may be different from that between the PS surface and water. From a theoretical perspective, charged surfaces have been reported to interact with counterions near the surface, and the velocity of fluids was reported to be suppressed by the Coulomb interaction.[30–32] The condition of $v = 0$ was suggested to be found away from the surface ($h > 0$).[30] Ideally, the particle surface is assumed

Figure 4 Change of the drag force with the change of the flow velocity for polystyrene (PS) particles of various sizes, as mentioned in the inset. As seen in this figure, due to the increase in particle size, the drag force on the PS particles also increased. The straight lines were drawn according to the least-squares fit method.

Table 1 Drag coefficient per unit size ($Fv^{-1}D^{-1}$) and zeta potentials of microparticles of different surface morphologies

Particle		$Fv^{-1}D^{-1} \times 10^{-3}$ (pN s µm^{-2})	Ratio	Zeta potential (mV)
Flat	PS	7.04 ± 0.32	1	-43.4
Grafted	PAAm-grafted	8.49 ± 2.10	1.2	-16.5
Rough	Silica	2.90 ± 1.74	0.4	-57.8
Hydrogel	PAMPS	1.01 ± 0.63	0.14	-41.7

Abbreviations: PAAm, polyacrylamide; PAMPS, PAAm–methylpropane sulfonic acid; PS, polystyrene.
Here F, v and D represent the drag force, the velocity of the particle and the diameter of the particle, respectively. The drag coefficients of the microparticles differed with the change in the surface morphology and the zeta potentials. The table provides detailed quantitative data that also reveal the role of the particle surface morphology in altering the drag coefficient with respect to the standard polystyrene particle. 'Ratio' indicates the relative change in the drag coefficient per unit size with respect to that of the PS particle. Error, s.d.

Figure 5 (**a**) Schematic representation of the surface morphologies of different microparticles and scanning electron microscopy images of: (i) polystyrene particle (PS); (ii) polyacrylamide (PAAm)-grafted particle; (iii) silica particle; and (iv) PAAm–methylpropane sulfonic acid (PAMPS) gel particle. (**b**) Effect of the surface morphology of the microparticles and the particle size on the drag coefficient per unit size. Here F, v and D represent the drag force, the velocity of the particle and the diameter of the particle, respectively. The surface morphology is observed to strongly affect the drag coefficient of the particles in the aqueous fluidic medium. Scale bars for (i), (ii) and (iii), 5 µm; for (iv), 1 µm.
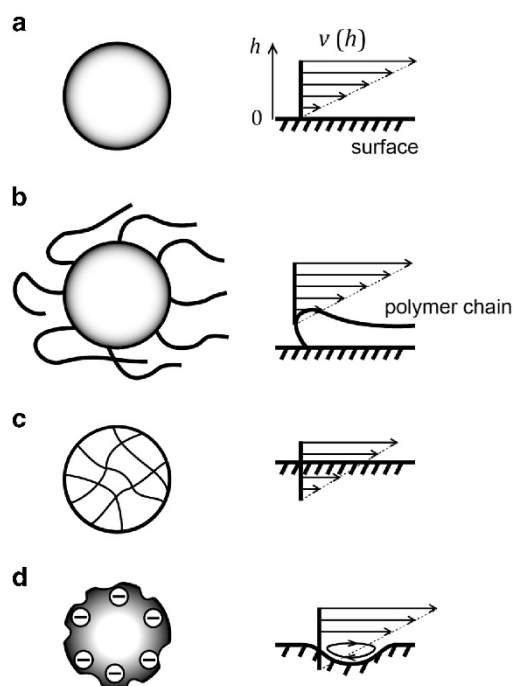
to be smooth, such as for a face-centered cubic solid surface. However, because the silica particle is amorphous, the same assumption is not maintained due to surface roughness, as schematically shown in the Figure 6d. Such a rough surface may result in the formation of local turbulent or counter flow of the buffer in the dips and decrease the surface friction, which is also indicated by our result. The rough and hairy surface morphologies are thus very difficult to treat theoretically

Figure 6 Schematic representation of microparticles with different surface morphologies in the flow channel (left) and distributions of the velocity in the vicinity of the particle surface (right) for: (**a**) a polystyrene particle with smooth surface, (**b**) a polyacrylamide (PAAm)-grafted particle, (**c**) a PAAm–methylpropane sulfonic acid hydrogel particle and (**d**) a silica particle with a negatively charged rough surface.

at boundary conditions because conventional theoretical studies on the drag force measurement of small particles have been performed under the assumption of a rigid surface as a boundary condition.[32–36] In our experiment, we measured the drag force on a small gel particle or a hairy particle, both of which have an unclear boundary with the surrounding medium. Therefore, we describe our results by using a phenomenological scheme, as discussed above.

CONCLUSIONS

In conclusion, we established an experimental setup for measuring the drag force acting on any microobject under fluid flow. Moreover, we investigated the role of surface morphology, size and the physical

nature of the object in altering the drag coefficient of the object. The drag coefficient was decreased by ~ 60 and ~ 86% for the negatively charged hard and soft spheres, respectively, whereas it increased by ~ 20% for the polymer-grafted PS particle with respect to that of the standard PS particle. To the best of our knowledge, very few reports are found in the literature regarding the alteration of drag force in the case of very small objects and the role of surface morphology in altering the drag force. Hence, our work is important for understanding the role of surface morphology in the alteration of the drag force acting on microparticles, especially with rough or hairy surface morphologies and different physical natures. This work might be helpful in elucidating the mechanism behind the change in the drag coefficient of aquatic microorganisms, which is closely related to their survival; in addition, this work may also have an important role in developing new technologies for future microdevices.

CONFLICT OF INTEREST

The authors declare no conflict of interest.

1 Howard, J. *Mechanics of Motor Proteins and the Cytoskeleton* (Sinauer Associates, Inc., Sunderland, MA, USA, 2001).
2 Lighthill, M. J. in *Scale Effects in Animal Locomotion* (ed. Pedley, T. J.) 365–404 (Academic Press, New York, NY, USA, 1977).
3 Rayner, J. M. V. in *Scale Effects in Animal Locomotion* (ed. Pedley, T. J.) 437–443 (Academic Press, New York, NY, USA, 1977).
4 Ward-Smith, A. J. Analysis of the aerodynamic performance of birds during bounding flight. *Math. Biosci.* **68**, 137–147 (1984).
5 Bushnell, D. M. & Moore, K. J. Drag reduction in nature. *Annu. Rev. Fluid Mech.* **23**, 65–79 (1991).
6 Aleyev, Y. G. *Nekton* (Springer, The Netherlands, 1977).
7 Kozlov, L. F. & Shakalo, V. M. Certain results of the determination of pulsation of velocities in the boundary layer of dolphins. *Bionika* **7**, 37–40 (1973).
8 Ovchinnikov, V. V. in *Ecomorphological Research in Nektonic Animals* 42–52 (Naukova Dumka, Kiev, Ukraine, 1966).
9 Pershin, S. V., Chernyshov, L. F., Kozlov, L. F., Koval, A. P. & Zayets, V. A. Patterns in the integuments of fast-swimming fishes. *Bionika* **10**, 3–21 (1976).
10 Reif, W. E. Protective and hydrodynamic function of the dermal skeleton of Elasmobranchs. *N. Jb. Geol. Palaont. Abh.* **157**, 133–141 (1978).
11 Reif, W. E. Morphogenesis and function of the squamation in sharks. *N. Jb. Geol. Palaont. Abh.* **164**, 172–183 (1982).
12 Reif, W. E. & Dinkelacker, A. Hydrodynamics of the squamation in fast-swimming sharks. *N. Jb. Geol. Palaont. Abh.* **164**, 184–187 (1982).
13 Raschi, W. G. & Musick, J. A. *Hydrodynamic Aspects of Shark Scales*. Report No. NASA-CR-3963 (Langley Research Center Library, NASA, Hampton, VA, USA, 1986).
14 Pershin, S. V., Sokolov, A. S. & Tomilin, A. G. Regulated hydroelastic effect in the fins of the largest and fastest dolphin, the killer whale. *Bionika* **13**, 35–43 (1979).
15 Lewis, R. W. Fish cutaneous mucus: a new source of skin surface lipids. *Lipids* **5**, 947–949 (1970).
16 Mittal, A. K. & Agarwal, S. K. Histochemistry of the unicellular glands in relation to their physiological significance in the epidermis of *Monopterus-Cuchia* Synbranchiformer Pisces. *J. Zool.* **182**, 429–440 (1977).
17 Lebedeva, N. E. & Chernyakov, Y. L. Chemical danger signal in the predator-prey system among fish. *Zh. Evol. Biokhim. Fiziol.* **14**, 392–397 (1978).
18 Zaccone, G. Histochemistry of keratinization and epithelial mucins in the skin of the marine *Teleost Muraena Helena* L. Anguilliformer, Pisces. *Cell. Mol. Biol.* **24**, 37–50 (1979).
19 Ovchinnikov, V. V. Swordfishes and Billfishes in the Atlantic Ocean, ecology and functional morphology [Isr. Program for Sci. Transl.]. *Rep. Atl. Sci. Res. Inst. Fish. Oceanogr, Kalingrad* 1–77 (1971).
20 Povkh, I. L., Stupin, A. B. & Boyarkina, G. G. Hydrodynamic resistance of aqueous solutions of polymers and surface-active substances in rough tubes. *Inzh.-Fiz. Zh.* **36**, 16–19 (1979).
21 Thomson, B., Rudin, A. & Lajoie, G. Dispersion copolymerization of styrene and divinylbenzene. II. Effect of crosslinker on particle morphology. *J. Appl. Polym. Sci.* **59**, 2009–2028 (1996).
22 Kawguchi, H., Isono, Y. & Tsuji, S. Hairy particles prepared by living radical graft-polymerization. *Macromol. Symp.* **179**, 75–88 (2002).
23 Tsuda, Y., Shimizu, T., Yamato, M., Kikuchi, A., Sasagawa, T., Sekiya, S., Kobayashi, J., Chen, G. & Okano, T. Cellular control of tissue architectures using a three-dimensional tissue fabrication technique. *Biomaterials* **28**, 4939–4946 (2007).
24 Jo, B. H., Van Lerberghe, L. M., Motsegood, K. M. & Beebe, D. J. Three-dimensional micro-channel fabrication in polydimethylsiloxane (PDMS) elastomer. *J. Microelectromech. Syst.* **9**, 76–81 (2000).
25 Eom, N., Stevens, V., Wedding, A. B., Sedev, R. & Connor, J. N. Probing fluid flow using the force measurement capability of optical trapping. *Adv. Powder Technol.* **25**, 1249–1253 (2014).
26 Sasaki, K, Tsukima, M. & Masuhara, H. Three-dimensional potential analysis of radiation pressure exerted on a single microparticle. *Appl. Phys. Lett.* **71**, 37–39 (1997).
27 Sasaki, K., Hotta, J. I., Wada, K. I. & Masuhara, H. Analysis of radiation pressure exerted on a metallic particle within an evanescent field. *Opt. Lett.* **25**, 1385–1387 (2000).
28 Wada, K., Sasaki, K. & Masuhara, H. Optical measurement of interaction potentials between a single microparticle and an evanescent field. *Appl. Phys. Lett.* **76**, 2815–2817 (2000).
29 Wada, K, Sasaki, K. & Masuhara, H. Electric charge measurement on a single microparticle using thermodynamic analysis of electrostatic forces. *Appl. Phys. Lett.* **81**, 1768–1770 (2002).
30 Joly, L., Ybert, C., Trizac, E. & Bocquet, L. Hydrodynamics within the electric double layer on slipping surfaces. *Phys. Rev. Lett.* **93**, 257805-1–257805-4 (2004).
31 Kim, Y. W. & Netz, R. R. Electro-osmosis at inhomogeneous charged surfaces: hydrodynamic versus electric friction. *J. Chem. Phys.* **124**, 114709-1–114709-21 (2006).
32 Joly, L., Ybert, C., Trizac, E. & Bocquet, L. Liquid friction on charged surfaces: from hydrodynamic slippage to electrokinetics. *J. Chem. Phys.* **125**, 204716-1–204716-14 (2006).
33 van Zessen, E., Tramper, J., Rinzema, A. & Beeftink, H. H. Fluidized-bed and packed-bed characteristics of gel beads. *Chem. Eng. J.* **115**, 103–111 (2005).
34 Chassagne, C. & Koper, G. J. M. Electrically induced anisotropy in nanospheres dispersions. *Physica A* **298**, 24–31 (2001).
35 Landau, L. D. & Lifshitz, E. M. *Fluid Mechanics* 2nd edn (Butterworth-Heinemann, Boston, MA, USA, 1988).
36 Norman, A. *Effect of Surface Morphological Changes on Flow Over a Sphere*. PhD dissertation, California Institute of Technology (2010).